INSTITUTE OF PHYSICS PUBLISHING JOURNAL OF PHYSICS D: APPLIED PHYSICS

J. Phys. D: Appl. Phys. **36** (2003) 2878–2882 PII: S0022-3727(03)59809-6

Micro electron bunch generation by intense short pulse laser

Shuji Miyazaki[1], **Qing Kong**[1], **Shigeo Kawata**[1] **and Jiri Limpouch**[2]

[1] Department of Electrical and Electronic Engineering, Utsunomiya University, Yohtoh 7-1-2, Utsunomiya 321-8585, Japan

[2] Institute of Physics/Czech Technical University, Academy of Sciences of the Czech Republic, CZ-182 121 Praha 8, Czech Republic

E-mail: kwt@cc.utsunomiya-u.ac.jp

Received 20 February 2003
Published 19 November 2003
Online at stacks.iop.org/JPhysD/36/2878

Abstract

The generation of a high-energy electron bunch is studied by using an intense fs TEM(1, 0) mode laser in vacuum. We perform three-dimensional particle simulations in which the relativistic equation of motion is solved with an analytically expressed laser field. In this paper, we found that electrons are accelerated longitudinally and confined in the transverse direction by a ponderomotive force of an intense short pulse TEM(1, 0) mode laser. Using a TEM(1, 0) mode laser of 10^{17} W cm^{-2}, the electrons are successfully trapped in the polarized direction and accelerated to the order of tens of megaelectronvolts with an acceleration gradient of about gigaelectronvolts per metre. The electron bunch generated has a small emittance in the transverse and longitudinal directions, and the spatial size of the electron bunch is about several hundred micrometres in each direction with a high electron number density. This electron acceleration mechanism may open a new engineering world towards a point radiation source, a precise measurement, applications to material sciences, and so on.

1. Introduction

In recent years, we have seen the developments of intense laser and laser pulse length compression with the invention of the chirped pulse amplification (CPA) technique [1]. The CPA laser can make the intensities larger than $\sim 10^{21}$ W cm^{-2} with short pulses. Such lasers allowed pioneering new research areas in electron acceleration [2–6]. Among them, we study the generation of a high-energy and high-density micro electron bunch using a high-intensity short-pulse TEM(1, 0) mode laser in vacuum. The electron motion can be divided into a high-frequency quiver and a drift motion. The quiver motion is a result of the laser oscillation. The drift is cased by the ponderomotive force, which is generated by a nonlinear effect. The ponderomotive force is proportional to the gradient of the laser field energy density. At the high-intensity laser ($a_0 \geqslant 0.1$–1.0) focused on the electrons, the strong ponderomotive force pushes the electrons to the direction opposite the gradient of the laser intensity. Here $a_0 = eE_0/m_e\omega c$ is a dimensionless parameter of the laser field intensity, e and m_e are the electron charge and rest mass, respectively, ω is the laser angular frequency, E_0 is the amplitude of the electric field and c is the speed of light in vacuum. On the other hand, the focused laser also has a field gradient in the radial direction. The transverse ponderomotive force may scatter electrons in the radial direction [7, 8]. The TEM(0, 0) mode laser, which is widely used, has an intensity peak at the central axis. Therefore, the electrons receive the strong ponderomotive force to the transverse direction with the oscillation in the polarized direction. Therefore, the electrons scatter to the polarized direction strongly and the quality of the electron bunch accelerated is degraded. The main purpose of this study is to suppress the scattering in the polarized direction and to generate a high-energy and high-density micro electron bunch. We adopt a TEM(1, 0) mode laser [9] in order to suppress the electron scattering to the polarized direction. The TEM(1, 0) mode laser has two peaks in the polarized direction. The electrons are accelerated near the laser focal point and confined between the two intensity peaks in the

polarized direction by the transverse ponderomotive force. Consequently, a high-quality electron bunch can be generated.

In section 2, we describe our simulation model and parameter set. In section 3, simulation results are presented and the quality of the accelerated electron bunch is investigated. In section 4, conclusions are described.

2. Simulation model

Figure 1 shows the schematic view of electron acceleration by an intense short-pulse TEM(1, 0) mode laser. The width of an injected electron bunch (l_x, l_y, l_z) is $(2w_0, 2w_0, 8L_z)$. Here, w_0 and L_z are the laser minimal spot size and the pulse length, respectively. The electron bunch moves to the z-direction at a speed of $0.95c$. At the initial time, t_{begin}, the injected electron bunch does not interact with the laser pulse. The centres of the laser pulse and the electron bunch coincide with each other at the focal point, $(x, y, z) = (0, 0, 0)$ at the time $t = 0$. The laser wavelength, λ, is $1.053\,\mu$m, the laser intensity $10^{17}\,\mathrm{W\,cm^{-2}}$ ($a_0 \sim 0.2$), the laser pulse length 10λ, the minimal spot size 35λ and the number density of the initial electron bunch $5.48 \times 10^{10}\,\mathrm{cm^{-3}}$.

In our simulations, we give the laser field analytically and solve the relativistic motion of electrons numerically. A laser of TEM(1, 0) mode, which is linearly polarized in the x-direction and propagates along the z-direction, is used. The transverse components of the electric field are given by [9]

$$E_x = 2\sqrt{2}E_0\frac{w_0}{w(z)^2}x\exp\left[-\frac{r^2}{w(z)^2}-\frac{(z-ct)^2}{L_z^2}\right] \times \exp\left\{\mathrm{i}\left[kz-\omega t-2\phi(z)+\frac{kr^2}{2R(z)}\right]\right\}, \tag{1}$$

$$E_y = 0, \tag{2}$$

where

$$r^2 = x^2 + y^2, \tag{3}$$

$$w(z) = w_0\left[1+\left(\frac{z}{z_{\mathrm{R}}}\right)^2\right]^{1/2}, \tag{4}$$

$$R(z) = z\left[1+\left(\frac{z_{\mathrm{R}}}{z}\right)^2\right], \tag{5}$$

$$\phi(z) = \tan^{-1}\left(\frac{z}{z_{\mathrm{R}}}\right). \tag{6}$$

Here, $z_{\mathrm{R}} = \pi w_0^2/\lambda$ is the Rayleigh length. The other electric and magnetic components are obtained by the paraxial approximation [10–12]

$$E_z = \frac{\mathrm{i}}{k}\frac{\partial E_x}{\partial x}, \tag{7}$$

$$\boldsymbol{B} = -\frac{\mathrm{i}}{\omega}\nabla\times\boldsymbol{E}. \tag{8}$$

The paraxial approximation is used to obtain the analytical formula of the laser field. The accuracy of this approximation is related to the minimal spot size of the laser. When $kw_0 \geqslant 50$, this approximation is accurate enough to describe the electron–laser interaction [12].

For an electron moving in an ultra-intense laser field, the electron radiation damping effect should be considered. The radiation damping force is written by

$$\boldsymbol{f} = -\frac{2e^4}{3m_{\mathrm{e}}^2c^5}\gamma^2\boldsymbol{v}\left[\left(\boldsymbol{E}+\frac{1}{c}\boldsymbol{v}\times\boldsymbol{B}\right)^2-\frac{1}{c^2}(\boldsymbol{E}\cdot\boldsymbol{v})^2\right]. \tag{9}$$

This relativistic approximation for $\boldsymbol{f}$ is valid for the relativistic electron velocity and laser intensity. The relativistic equation of motion including the radiation damping effect is given by

$$\frac{\mathrm{d}\boldsymbol{P}}{\mathrm{d}t} = -e\left(\boldsymbol{E}+\frac{1}{c}\boldsymbol{v}\times\boldsymbol{B}\right)+\boldsymbol{f}. \tag{10}$$

Here, $\boldsymbol{P}$ and $\boldsymbol{v}$ are the momentum and velocity of the electron, respectively. γ is the relativistic factor of the electron. For the parameters we employ in this paper, the electron radiation damping effect is weak. The interaction among the electrons is also weak. The validity of these assumptions is proved in section 3. The Buneman scheme [13], which is widely used in particle simulations and has a second-order accuracy in space and time, is employed to solve equation (10).

3. Simulation results

The incident electron bunch interacts with the laser pulse near the focal point. When the laser pulse reaches the focal point, the electrons, which exist near the intensity peaks, are accelerated well to the z-direction according to the strong ponderomotive force in the z-direction. Figures 2(a) and (b) represent distributions of the final electron relativistic factor γ

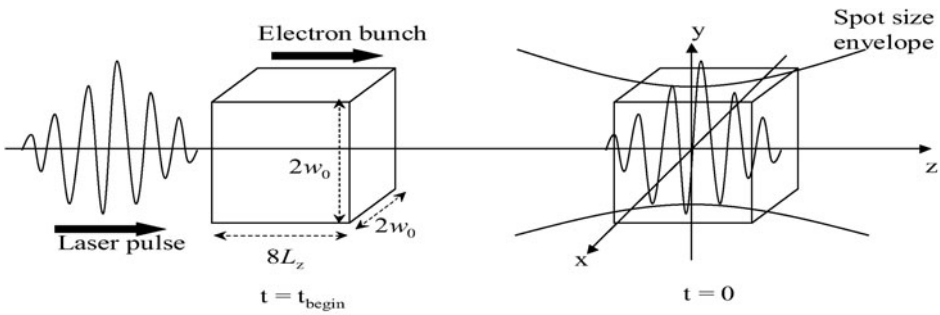

Figure 1. Schematic view of the simulation model of the electron acceleration in vacuum by the intense short-pulse TEM(1, 0) mode laser. The laser and injected electron bunch propagate along the laser axis. Here, w_0 is the minimal spot size of the laser and L_z is the laser pulse length. The left-side view shows the state of the laser and an electron bunch at the time t_{begin}. We set the centres of the laser and electron bunch to coincide with each other at the time $t = 0$.

at $t_{\rm final}$ in the x–z plane and the y–z plane, respectively. Here $t_{\rm final} = 30\,000\lambda/c$. Figure 2($a$) shows that the electrons are accelerated to the z-direction and the accelerated electrons are gathered around the central axis. The laser is polarized in the x-direction. The electrons oscillate by the electric field in the polarized direction and the transverse ponderomotive force works in the x- and y-directions. The electric field, E_y, is zero in the TEM(1, 0) mode laser. Therefore, the electrons are not scattered much in the y-direction compared with the electrons scattering in the x-direction as shown in figure 2(b). Figure 3 shows the averaged electron number density distribution in the x–z plane at $t_{\rm final}$. The number density is averaged in the y-direction. The number density peak of electrons appears around $x = 0$ and $z = 30\,000\lambda$. The maximum number density of accelerated electrons is about $2.70 \times 10^8\,{\rm cm}^{-3}$ and the maximum energy density is about $5.39\,{\rm PeV\,cm}^{-3}$. Consequently, the accelerated electrons are confined between the intensity peaks in the x-direction, and the high-density high-energy electron bunch is generated as shown in figures 2 and 3. Figure 4(a) shows trajectories of most accelerated electrons (CASE1) and other scattered electrons (CASE2) in the x–z plane. Figure 4(b) corresponds to the electron energy change along the laser axis for these electrons. The initial position of the CASE1 electron is near the peak of laser intensity in the x-direction. In CASE2, the electron is initially located slightly outside the peak of laser intensity. The CASE1 electron is accelerated well successively near the focal point and captured by the laser field along the laser axis. On the other hand, the CASE2 electron receives a strong scattering by the laser pulse near the focal point and does not absorb the laser wave energy well. The ponderomotive force in the x-direction for the CASE1 electron near the focal point is small compared with that in a CASE2. Therefore in CASE2 the strong ponderomotive force pushes the CASE2 electron far from the laser axis in the x-direction before sufficient acceleration. The final electron energy, $E_{\rm max}$, in CASE1 is about 39.9 MeV with an acceleration gradient of $5.55\,{\rm GeV\,m}^{-1}$.

In order to make the acceleration mechanism clear, we compare the motion of the two electrons. We use an energy equation, $\mathrm{d}(m_{\rm e}c^2\gamma)/\mathrm{d}t = -e\boldsymbol{v}\cdot\boldsymbol{E}$, and a time-averaged ponderomotive force, which is given by [14]

$$F_{\rm pond}(t) = -\nabla V_{\rm pond}(x, y, z, t), \tag{11}$$

$$V_{\rm pond}(x, y, z, t) = \left[\left(1 + \frac{a^2(x, y, z, t)}{2}\right)^{1/2} - 1\right] m_{\rm e}c^2. \tag{12}$$

Here, $a^2/2$ is the normalized time-averaged laser intensity, which is written as

$$a^2(x, y, z, t) = 8a_0^2 \frac{w_0^2}{w(z)^4} x^2 \exp\left[-\frac{2r^2}{w(z)^2} - \frac{2(z - ct)^2}{L_z^2}\right]. \tag{13}$$

The work and the ponderomotive force acting on the two electrons are shown in figure 5. Figures 5(a1) and (a2) show the electron energy, γ, versus z. Figures 5(b1), (c1), (b2) and (c2) present the x and z components of the energy equation. Figures 5(d1), (e1), (d2) and (e2) represent the x and z components of the ponderomotive force as a function

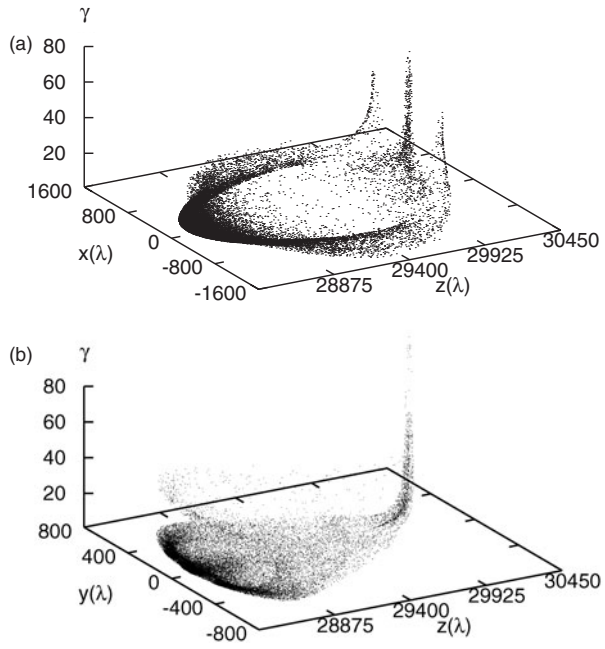

Figure 2. The electron energy, γ, maps in (a) the x–z plane and (b) the y–z plane at $t_{\rm final}$.

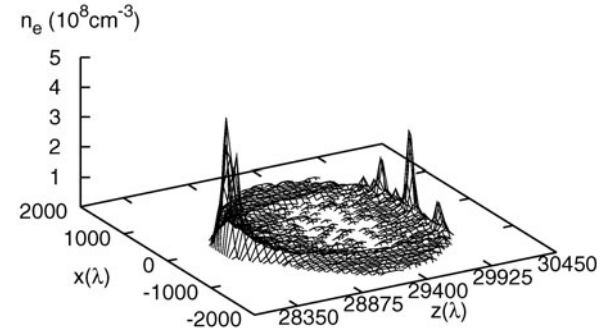

Figure 3. The electron number density, $n_{\rm e}$, distribution in the x–z plane at $t_{\rm final}$.

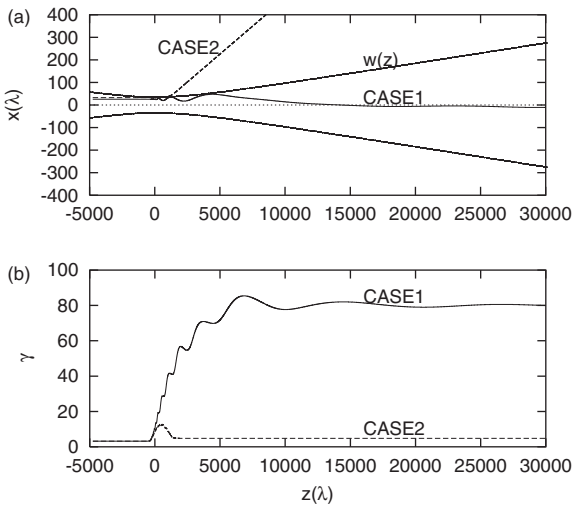

Figure 4. (a) The electron trajectories in the x–z plane. (b) The electron energy γ versus z. Here $w(z)$ represents the laser spot size envelope. The CASE1 shows the most accelerated electron and the CASE2 shows the scattered electron.

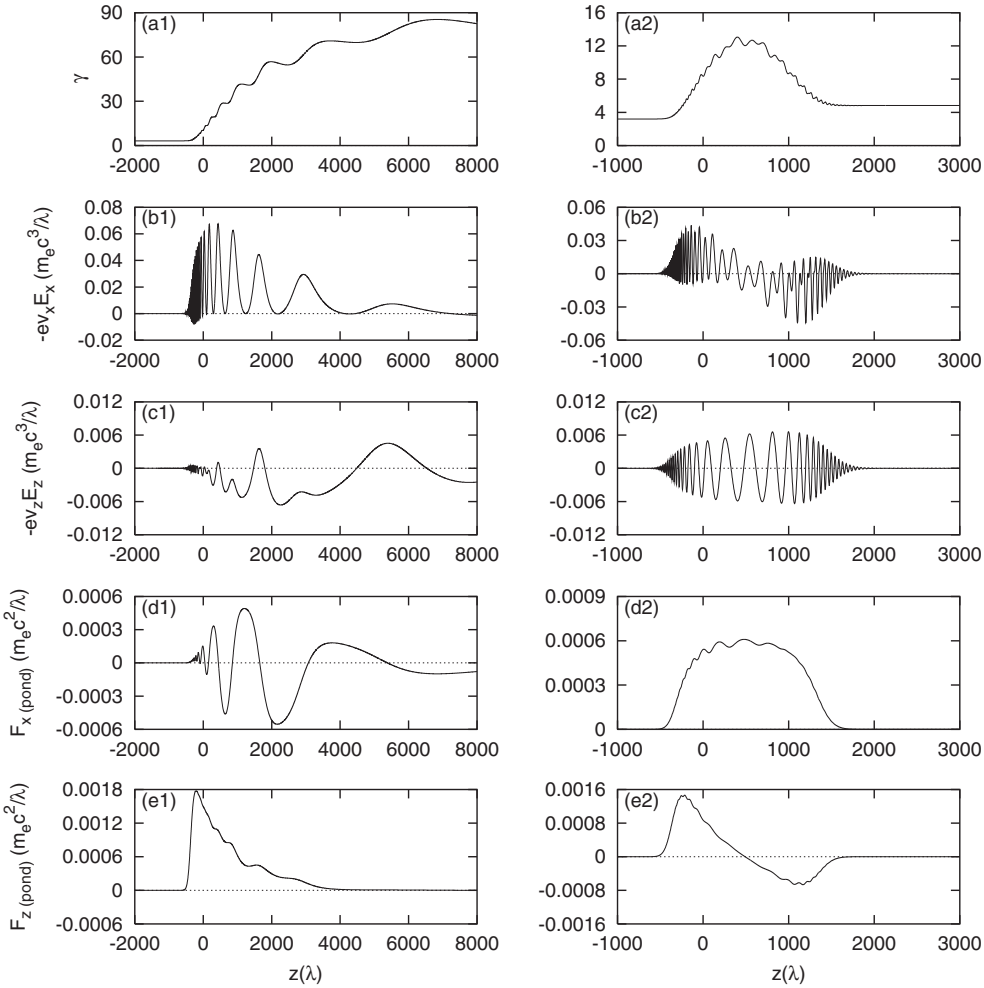

Figure 5. The work and the ponderomotive force acting on the electrons versus z. The left side shows the well-accelerated electron (CASE1) and the right presents the scattered electron (CASE2). ($a1$) and ($a2$) represent the variation of the electron energy, γ, near the focus, ($b1$), ($b2$), ($c1$) and ($c2$) show the work in the x- and z-directions as a function of z, based on the energy equation, and ($d1$), ($d2$), ($e1$) and ($e2$) represent the time-averaged ponderomotive forces in the x- and z-directions as a function of z.

of z. As shown in figures 5($b1$), ($c1$), ($b2$) and ($c2$) the longitudinal electric field, E_z, is much smaller than the transverse electric field, E_x. Therefore, the longitudinal component of the energy equation, $-ev_zE_z$, influences the energy variation in neither CASE1 nor CASE2. Therefore, the energy change in the electrons is governed mainly by the x component of the energy equation, $-ev_xE_x$. In CASE1 the electron receives the laser energy in the vicinity of the focal point. On the other hand, the CASE2 electron cannot absorb the wave energy. The ponderomotive force works in the direction opposite the gradient of the laser intensity. The CASE1 electron is located near the laser intensity peak in the x-direction near the focal point. From figures 5($d1$) and ($e1$), the CASE1 electron has nearly no influence from the gradient of the intensity in the x-direction near the focal point. The CASE1 electron is accelerated successively. Because of the effective acceleration in CASE1, the difference in phase velocity between the electron and laser pulse becomes small. Therefore, the CASE1 electron is sitting for a long time in front of the laser pulse. When the CASE1 electron moves behind the laser pulse peak, the laser expands, its intensity becomes weak and the ponderomotive force becomes small. In figures 5($d2$) and ($e2$) the initial position of the CASE2 electron is located just outside the laser intensity peak, and the ponderomotive force pushes the electron quickly outwards in the x-direction. As a result, the CASE2 electron slips out of the laser pulse and loses its energy.

Figures 6(a) and (b) show the enlarged electron bunch maps in the x–z and y–z planes at t_{final}, respectively. The size of the accelerated electron bunch is 100–200λ in the x-direction, 100–150λ in the y-direction and 30–50λ in the z-direction. The transverse and longitudinal rms emittances, which measure the quantity of the accelerated electron bunch, are shown by [8,15]

$$\epsilon_x = \{\overline{(x-\bar{x})^2}\,\overline{(x'-\bar{x}')^2} - [\overline{(x-\bar{x})(x'-\bar{x}')}]^2\}^{1/2}, \qquad (14)$$

$$\epsilon_z = \tilde{z}\frac{\Delta\tilde{P}_z}{P_0}. \qquad (15)$$

Here $x' = \mathrm{d}x/\mathrm{d}z$ is the slope of the electron trajectory, $z = s(t) - s_0(t)$ is the difference in the direction the beam propagation, $\Delta P_z = P_z - P_0$ is the difference in the momentum in the longitudinal direction. $s(t)$ is the distance of transfer along the direction of beam propagation. P_z and P_0 are the longitudinal momentum and the averaged value of the longitudinal momentum, respectively. The rms emittances of

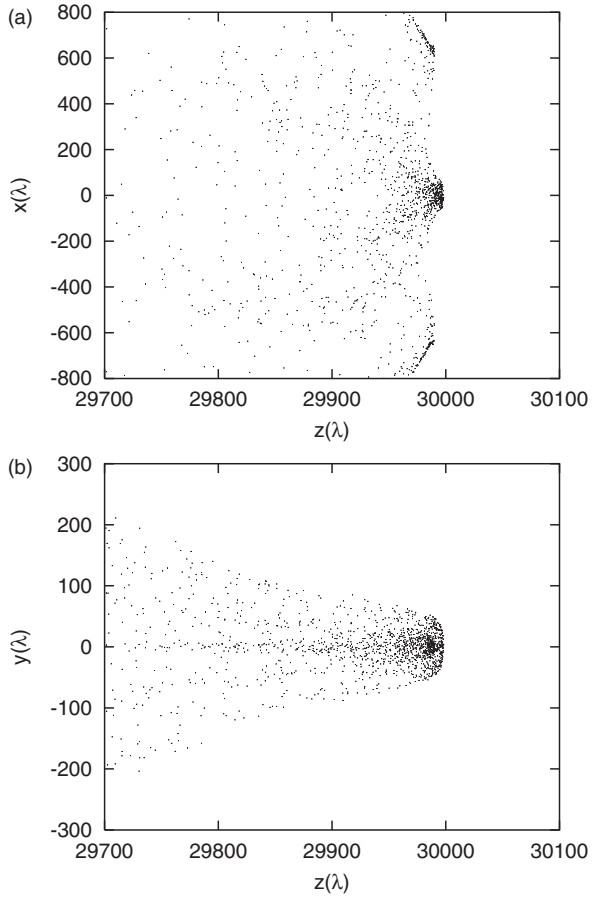

Figure 6. The enlarged electron bunch maps in (*a*) the x–z and (*b*) the y–z planes.

the electron bunch accelerated in the x-, y- and z-directions ($\epsilon_x, \epsilon_y, \epsilon_z$) are about 0.322, 1.54×10^{-3} and 5.23 mm mrad. The averaged energy of the accelerated electron bunch is about 18.6 MeV and the averaged number density is about $0.835 \times 10^8\,\mathrm{cm}^{-3}$.

In our simulations, the electron–electron interaction is neglected. Here, the limit of the accelerated electron number, under which the interaction between the accelerated electrons is negligible, is estimated. It is given by [8]

$$N < \frac{w(z)}{r_\mathrm{e}} \left(\frac{P_\perp}{m_\mathrm{e} c} \right)^2 . \tag{16}$$

Here, N is the limit of the accelerated electrons number, r_e is the classical electron radius and $P_\perp$ is the transverse momentum of accelerated electrons. As a result, the limit number of the accelerated electrons, N, is about 4.82×10^7 and it corresponds to the number density $\sim 10^{11}\,\mathrm{cm}^{-3}$. The maximum accelerated electrons number density in our simulations is about $2.70 \times 10^8\,\mathrm{cm}^{-3}$, and we can ignore the electron–electron interaction. The accelerated electron also receives the acceleration and radiates the energy partly. The expression of the total radiation energy is written as

$$E_\mathrm{radiation} = \frac{2e^4}{3m_\mathrm{e}^2 c^3} \int_{-\infty}^{\infty} \gamma^2 \left[\left(\boldsymbol{E} + \frac{1}{c^2} \boldsymbol{v} \times \boldsymbol{H} \right)^2 - \frac{1}{c^2} (\boldsymbol{E} \cdot \boldsymbol{v})^2 \right] \mathrm{d}t . \tag{17}$$

The total radiation energy of the most accelerated electron is about 0.201 eV. Therefore, $E_\mathrm{radiation}/E_\mathrm{max} \sim 1.99 \times 10^{-8}$ and the radiation damping effect is also negligible.

4. Conclusions

We studied high-energy and high-density micro electron bunch generation using the intense short-pulse TEM(1, 0) mode laser. The electrons are accelerated by the longitudinal ponderomotive force near the focal point and captured by the laser field without scattering to the polarized direction. During the laser–electron interaction, the electrons accelerated are focused around the central axis by the ponderomotive force in the polarized direction. The size of the electron bunch accelerated is smaller than 200λ in the transverse direction and 30–50λ in the longitudinal direction. The number density of the accelerated electron bunch is $\sim 10^8\,\mathrm{cm}^{-3}$. The rms emittance in the transverse and longitudinal directions are of the order of millimetre milliradians. The electron energy reaches a few tens of megaelectronvolts with an acceleration gradient of about gigaelectronvolts per metre. The production of such an electron bunch may open a new field for point light sources or a new EUV source or applications in nano-technologies or particle acceleration schemes [16].

Acknowledgments

This work is partly supported by JSPS (Japan Society for the Promotion of Science) and also by the KEK cooperation research program conducted by Prof. Kurokawa and Prof. Nakajima in KEK. We would like to present our thanks also to Prof. Y K Ho, Prof. Mima, Prof. Miyanaga, Prof. Pogorelsky and Prof. Yakimenko for fruitful discussions with them on this subject.

References

[1] Mourou G A and Tajima T 2001 *Proc. Inertial Fusion Sciences and Applications 2001* (Paris: Elsevier) p 831
[2] Scully M O and Zubairy M S 1991 *Phys. Rev.* A **44** 2656
[3] Hafizi B, Ting A, Esarey E, Sprangle P and Krall J 1997 *Phys. Rev.* E **55** 5924
[4] Kong Q, Ho Y K, Wang J X, Wang P X, Feng L and Yuan Z S 2000 *Phys. Rev.* E **61** 1981
[5] Cheng Y and Xu Z 1999 *Appl. Phys. Lett.* **74** 2116
[6] Malka G, Lefebvre E and Miquel J L 1997 *Phys. Rev. Lett.* **78** 3314
[7] Chaloupka J L and Meyerhofer D D 1999 *Phys. Rev. Lett.* **83** 4538
[8] Stupakov G V and Zolotorev M S 2001 *Phys. Rev. Lett.* **86** 5274
[9] Yariv A 1985 *Optical Electronics* 3rd edn (New York: CBS College Publishing) p 35
[10] Lax M, Louisell W H and McKnight W B 1975 *Phys. Rev.* A **11** 1365
[11] Davis L W 1979 *Phys. Rev.* A **19** 1177
[12] Cao N, Ho Y K, Kong Q, Wang P X, Yuan X Q, Nishida Y, Yugami N and Ito H 2002 *Opt. Commun.* **204** 7
[13] Buneman O 1967 *J. Comput. Phys.* **1** 517
[14] Wang P X *et al* 2002 *J. Appl. Phys* **91** 856
[15] Reiser M 1994 *Theory and Design of Charged Particle Beams* (New York: Wiley-Interscience) p 57
[16] Nakamura T and Kawata S 2003 *Phys. Rev.* E **67** 026403